Structural Basis for the Inhibition of Human 5,10-Methenyltetrahydrofolate Synthetase by N10-Substituted Folate Analogues

Dong Wu,[1] Yang Li,[1] Gaojie Song,[1] Chongyun Cheng,[1] Rongguang Zhang,[2] Andrzej Joachimiak,[2] Neil Shaw,[1] and Zhi-Jie Liu[1]

[1]National Laboratory of Biomacromolecules, Institute of Biophysics, Chinese Academy of Sciences, Beijing, China and [2]Structural Biology Center, Argonne National Laboratory, Argonne, Illinois

Abstract

5,10-Methenyltetrahydrofolate synthetase (MTHFS) regulates the flow of carbon through the one-carbon metabolic network, which supplies essential components for the growth and proliferation of cells. Inhibition of MTHFS in human MCF-7 breast cancer cells has been shown to arrest the growth of cells. Absence of the three-dimensional structure of human MTHFS (hMTHFS) has hampered the rational design and optimization of drug candidates. Here, we report the structures of native hMTHFS, a binary complex of hMTHFS with ADP, hMTHFS bound with the N5-iminium phosphate reaction intermediate, and an enzyme-product complex of hMTHFS. The N5-iminium phosphate captured for the first time in our crystal structure unravels a unique strategy used by hMTHFS for recognition of the substrate and provides structural basis for the regulation of enzyme activity. Binding of N10-substituted folate analogues places Y152 in the middle of the channel connecting ATP binding site with the substrate binding pocket, precluding the positioning of γ-phosphate for a nucleophilic attack. Using the structures of hMTHFS as a guide, we have probed the role of residues surrounding the active site in catalysis by mutagenesis. The ensemble of hMTHFS structures and the mutagenesis data yield a coherent picture of the MTHFS active site, determinants of substrate specificity, and new insights into the mechanism of inhibition of hMTHFS. [Cancer Res 2009;69(18):7294–301]

Introduction

The folate-dependent one-carbon metabolic network supplies carbon for the synthesis of purines, thymidine, and amino acids (Fig. 1; refs. 1, 2). Because these components are essential for the growth and proliferation of cells, the folate-dependent one-carbon metabolic network is a prime target for the development of anticancer therapeutics (3, 4). Several enzymes functioning in the network have been targeted successfully for the treatment of carcinomas. Methotrexate, one of the most successful antifolate to be administered in cancer chemotherapy (5), inhibits a key enzyme of the one-carbon metabolic network, dihydrofolate reductase, which catalyzes the conversion of dihydrofolate to tetrahydrofolate. Similarly, colorectal and pancreatic cancers are routinely treated by administration of the pyrimidine analogue 5-fluorouracil (5-FU), which inhibits thymidylate synthase (TS; ref. 6). TS converts deoxyuridylate to deoxythymidylate using a carbon donated by 5,10-methylenetetrahydrofolate (Fig. 1). This conversion is essential for DNA synthesis (7). To increase the clinical efficiency of the treatment, 5-formyltetrahydrofolate is often coadministered along with 5-FU. The beneficial effect of administering 5-formyltetrahydrofolate during the therapy with 5-FU is a consequence of the 5,10-methenyltetrahydrofolate synthetase (MTHFS)–catalyzed conversion of 5-formyltetrahydrofolate to 5,10-methenyltetrahydrofolate, which is further metabolized to 5,10-methylenetetrahydrofolate (Fig. 1). Lower levels of 5,10-methylenetetrahydrofolate have been shown to increase the dissociation of 5-FU from the ternary complex of TS and decrease the effectiveness of the pyrimidine analogue (8, 9). 5,10-Methylenetetrahydrofolate is also synthesized by serine hydroxymethyltransferase (SHMT) during conversion of serine to glycine. The activity of SHMT is regulated indirectly by MTHFS because the substrate of MTHFS, 5-formyltetrahydrofolate, inhibits SHMT (10–12). Glycinamide ribonucleotide transformylase and phosphoribosylaminoimidazolecarboxamide transformylase, two other enzymes of the one-carbon network, use carbons from 10-formyltetrahydrofolate for the synthesis of purines and have also been targeted for the treatment of carcinomas (13, 14).

MTHFS catalyzes the initial irreversible conversion of 5-formyltetrahydrofolate to 5,10-methenyltetrahydrofolate (15). The reaction is ATP dependent and is subject to feedback inhibition by the product (16–18). Previous studies using nuclear magnetic resonance spectroscopy and isotope exchange methods have shown that the reaction proceeds via the formation of two intermediates (19). A nucleophilic attack by the formyl group of 5-formyltetrahydrofolate on the γ-phosphate of ATP results in the formation of the first N5-iminium phosphate intermediate. This part of the reaction is reversible. The second nucleophilic attack is intramolecular and is mounted by N10 of the N5-iminium phosphate on N5, resulting in the formation of a tetrahedral intermediate—phosphoimidazolidine. Phosphoimidazolidine is eventually broken down to the product 5,10-methenyltetrahydrofolate by phosphate elimination. The last step of the reaction imparts irreversibility to the overall reaction catalyzed by MTHFS. To date, relatively little is known about the structural basis for the mechanism of catalysis. The crystal structures of a ternary complex of MTHFS from *Mycoplasma pneumoniae* (mpMTHFS) with ADP and 5-formyltetrahydrofolate (20) and a binary complex of MTHFS from *Bacillus anthracis* (bMTHFS) with ADP (21) have been

Note: Supplementary data for this article are available at Cancer Research Online (http://cancerres.aacrjournals.org/).

Requests for reprints: Zhi-Jie Liu or Neil Shaw, National Laboratory of Biomacromolecules, Institute of Biophysics, Chinese Academy of Sciences, Beijing 100101, China. Phone: 86-10-64857988; Fax: 86-10-64888426; E-mail: zjliu@ibp.ac.cn or neilshaw@moon.ibp.ac.cn.

doi:10.1158/0008-5472.CAN-09-1927

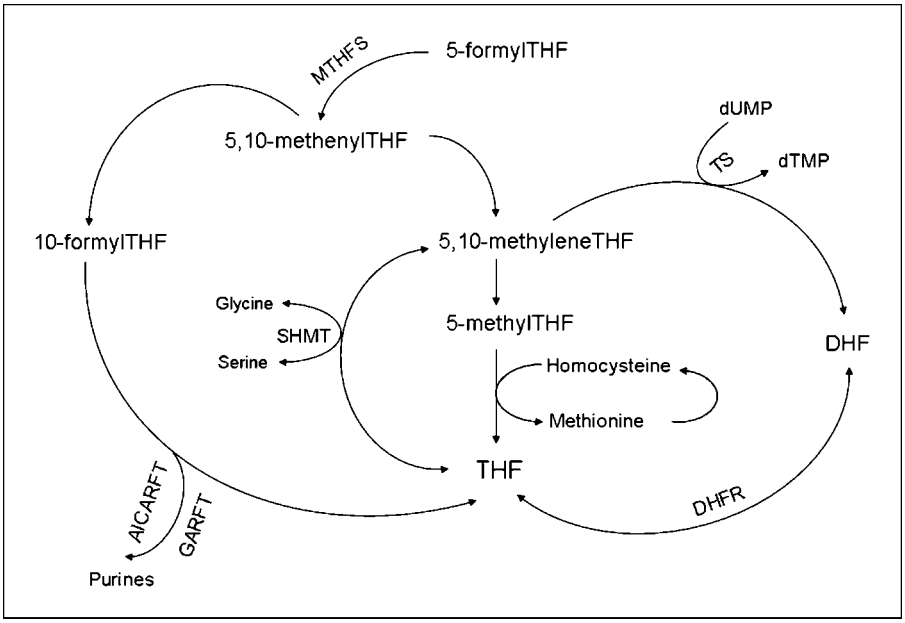

Figure 1. Diagrammatic representation of the one-carbon metabolic network. *DHF,* dihydrofolate; *DHFR,* dihydrofolate reductase; *THF,* tetrahydrofolate; *GARFT,* glycinamide ribonucleotide transformylase; *AICARFT,* phosphoribosylaminoimidazolecarboxamide transformylase.

reported. Although the ATP has been depicted as hydrolyzed and modeled as ADP and inorganic phosphate in the mpMTHFS structure, the substrate 5-formyltetrahydrofolate, rather than the product 5,10-methenyltetrahydrofolate, has been modeled in the active site. In addition, part of the 5-formyltetrahydrofolate moiety has been assigned zero occupancy. The overall structure of mpMTHFS and bMTHFS is similar, suggesting that MTHFS adopts a highly conserved fold. Attempts have been made to gain structural insights into inhibition of MTHFS based on steady-state kinetics and molecular modeling of a murine MTHFS (mMTHFS; refs. 22, 23). However, the interpretation of results is limited by the accuracy of the model of mMTHFS, which was generated by using a template that shares very low sequence identity.

Human MTHFS (hMTHFS) shares <28% sequence identity with structures of MTHFS homologues deposited in Protein Data Bank (PDB; ref. 24). In addition, several aspects of the structural basis for the mechanism of catalysis are unknown. What are the determinants of ligand specificity? Which residues are essential for catalysis? What is the structural basis for inhibition of hMTHFS by folate analogues? To begin to address these issues and provide a framework for the rational design of MTHFS inhibitors that could aid cancer chemotherapy, we have determined the structures of native hMTHFS, hMTHFS bound with ADP, hMTHFS in complex with an N5-iminium phosphate intermediate, and an enzyme-product complex of hMTHFS. Using the structures as a guide, essential residues have been mapped by site-directed mutagenesis. The structural and mutagenesis data unravel the determinants of substrate specificity and provide new insights into the mechanism of inhibition of hMTHFS.

Materials and Methods

Production of hMTHFS. *MTHFS* was amplified from human brain cDNA library using the following primers: 5′-TACTTCCAATCCAATGCTATGGCGGCGGCAGCGGT-3′ (forward) and 5′-TTATCCACTTCCAATGTTAAGCTGTTGACGAGTCT-3′ (reverse). The PCR product was ligated into pMCSG7 vector (25). Tobacco etch virus (TEV) protease-cleavable NH_2-terminal hexa His-tagged hMTHFS was produced in *Escherichia coli* BL21 DE3 cells. Cells were grown in Luria-Bertani medium at 37°C until the A_{600nm} reached 0.8. The culture was first cooled at 4°C for 45 min followed by induction at 16°C with 0.2 mmol/L isopropyl-L-thio-B-D-galactopyranoside for 20 h. Bacterial cells were harvested by centrifugation and lysed by sonication. Initial purification was carried out using Ni-affinity chromatography. His-tag was cleaved by treating the protein with TEV protease. Uncut protein and the TEV protease were removed by a second round of Ni-affinity chromatography. The protein was buffer exchanged into 20 mmol/L Tris-HCl (pH 8.0), 200 mmol/L NaCl, and 5 mmol/L β-mercaptoethanol using a Superdex G75 size exclusion column. After concentration, the protein (15–20 mg/mL) was immediately screened for crystallization.

MTHFS assay. The hMTHFS activity was measured by a Hitachi U-2010 spectrophotometer using [6*S*]-5-formyltetrahydrofolate (Sigma) as a substrate (23). hMTHFS was incubated with 0.5 mmol/L substrate in 400 μL of 50 mmol/L MES (pH 6.0), 20 mmol/L $MgCl_2$, and 5 mmol/L ATP at 30°C for 2 min. The amount of 5,10-methenyltetrahydrofolate formed at the end of incubation period was quantitated by measuring the absorbance at 360 nm. One unit of enzyme activity was defined as the amount of 5,10-methenyltetrahydrofolate formed per minute under the assay conditions. All assays were performed in triplicates under identical conditions with appropriate controls. The protein concentration was estimated by reading the absorbance at 280 nm. An extinction coefficient of 16,055 mol/L^{-1} cm^{-1} was used to calculate the amount of protein in mg/mL.

Site-directed mutagenesis. Mutagenesis was carried out using QuikChange site-directed mutagenesis kit (Stratagene) following the manufacturer's instructions. All the mutations were verified by sequencing the entire length of the clone. Mutant and wild-type hMTHFS were expressed, purified, and assayed under identical conditions.

Crystallization. Crystallization screening was done at 16°C using the Mosquito (TTP Lab Tech) crystallization robot. Hanging drops (0.6 μL) contained equal amounts of protein and mother liquor was equilibrated against 50 μL of reservoir solution. After screening 400 conditions of commercially available sparse matrix screens, crystals appeared within 2 d in a solution containing 100 mmol/L HEPES (pH 6.6), 20 mmol/L $MgCl_2 \cdot 6H_2O$, 20 mmol/L $NiCl_2 \cdot 6H_2O$, and 20% (w/v) PEG 3350. The crystals belonged to space group $C222_1$ with unit cell dimensions: a = 48.70 Å, b = 145.12 Å, c = 59.21 Å; α = 90.00°, β = 90.00°, γ = 90.00°.

Crystals for the binary complex of hMTHFS with ADP were obtained by mixing the protein with 5 mmol/L ATP before setting up crystallization drops. Crystals for the N5-iminium phosphate–bound hMTHFS and enzyme-product complex of hMTHFS were obtained by mixing the protein

with 5 mmol/L 5-formyltetrahydrofolate and 5 mmol/L ATP before setting up crystallization drops. Crystals harvested after 48 h revealed density for N5-iminium phosphate, whereas crystals harvested after 72 h contained the product 10-formyltetrahydrofolate in the active site. Crystals for all the complexes were obtained under the same conditions as that of the native hMTHFS.

Structure determination. Crystals were frozen in liquid nitrogen before diffraction testing and data collection. Native diffraction data were collected at a wavelength of 0.979 Å at beamline 19-ID [Advanced Photon Source (APS), Argonne National Laboratory]. Data were indexed and scaled to 1.9 Å resolution using HKL2000 (26). The structure was solved by molecular replacement with BALBES (27) using the structure of mpMTHFS (PDB code 1U3G) as a search model. The asymmetric unit consists of 1 molecule of MTHFS with a solvent content of 49.8%. Data for the complexes of hMTHFS were collected using an in-house FRE+ copper rotating anode and an R-AXIS IV^{++} detector (Rigaku). A 1.8 Å resolution data set for the enzyme-product complex was collected at APS. The structures of the complexes were solved by molecular replacement with Phaser (28) using the native structure as a search model. All the final models were refined using PHENIX refine (29) and Refmac (30). Five percent of the unique reflections were assigned in a random fashion to the "free" set for calculation of the free *R*-factor (*R*free); the remaining 95% of the reflections constituted the "working" set for the calculation of the *R*-factor (*R*; ref. 31). Manual adjustments to the model were done using COOT (32). Details of data collection and refinement statistics are listed in Supplementary Table S1. The quality of the final model was validated using MOLPROBITY (33).

The coordinates and structure factors of the native, ADP-bound, N5-iminium phosphate–bound, and 10-formyltetrahydrofolate–bound hMTHFS have been deposited in the PDB under the accession code 3HXT, 3HY6, 3HY4, and 3HY3, respectively.

Results

Overall structure of hMTHFS. The final model of the apoenzyme consists of 197 residues (Table 1). Six amino acids, L21-A23 and E187-D189, are disordered and could not be traced. The secondary structural elements of hMTHFS are arranged in a single domain with a three-layer, α/β/α, sandwich architecture and a topology similar to the Rossmann fold (Fig. 2*A* and *B*). The overall structure consists of a highly twisted sheet made up of eight β strands flanked by α helices on either side. hMTHFS is made up of five α helices. Whereas helices α2 and α3 are stacked against four parallel β strands at the center, α5 is seen stacked on the opposite side of the sheet. Interestingly, helix α1 is positioned almost perpendicular to α2 and is close to the edge of the sheet. Part of α1 is seen protruding out of the main body of the protein, suggesting that it may be involved in protein-protein interactions. The symmetry-generated intermolecular contacts introduced during crystal packing involve residues from α1. Helix α4 is seen inserted between strands β3 and β4, with a long loop connecting α4 with β4. Such an insertion is not observed in the structure of mpMTHFS. However, the overall structure of MTHFS from different sources is similar.

To gain insights into the architecture of the ATP binding site, hMTHFS was mixed with ATP before setting up crystallization drops. Electron density for the purine ring and the sugar moiety of the ATP was weak and only the phosphates could be modeled accurately (Fig. 2*A* and *C*). In the crystal structures of mpMTHFS and bMTHFS, the adenosine and sugar are lying on the surface and have very little contact with the protein. On the other hand, the phosphates are buried deep inside the protein and are involved in extensive ionic interactions. The structure of hMTHFS bound with phosphates (referred to as ADP-bound hMTHFS) is almost identical to the structure of the apoenzyme. The ATP used for cocrystallization experiments has been hydrolyzed to ADP and inorganic phosphate, as a result of which a diphosphate and an inorganic phosphate have been modeled in the structure. Residues E187-D189, which could not be traced in the structure of the apoenzyme, are well ordered in the structure of ADP-bound hMTHFS. These residues are close to the ATP binding site, with D189 forming a hydrogen bond with the O1 oxygen atom of the α-phosphate and a coordinate bond with the magnesium atom. In addition, D189 is now forming a salt bridge with K10. These new interactions observed in the structure of hMTHFS in complex with ADP help stabilize

Table 1. Relative activities of hMTHFS mutants

Mutation	Location	Relative activity (%)	Conservation
K10A	ATP binding site	7.5	Highly conserved
R14A	ATP binding site	12.9	Highly conserved
R145A	ATP binding site	2.3	Absolutely conserved
D154A	ATP binding site	0.9	Absolutely conserved
F55A	Close to pterin ring	53.6	Conserved
M58A	Close to pterin ring	121.6	None
E61A	Close to pterin ring	8.6	Absolutely conserved
Y83A	Close to pterin ring	100	None
M90A	Close to pterin ring	49.2	Conserved
Y152A	Close to pterin ring	24.9	Highly conserved
Y153A	Close to pterin ring	3.2	Absolutely conserved
F85A	Close to pABA ring	72.3	None
W109A	Close to pABA ring	39.7	None
R148A	Close to pABA ring	30.7	None
K150A	Close to pABA ring	100	None
Wild-type		100	

NOTE: Level of conservation has been assigned according to Clustal W convention (37). The top 100 sequences of MTHFS homologues obtained by running a PSI-BLAST search were curated by removing hypothetical and redundant sequences and aligned using Clustal W.

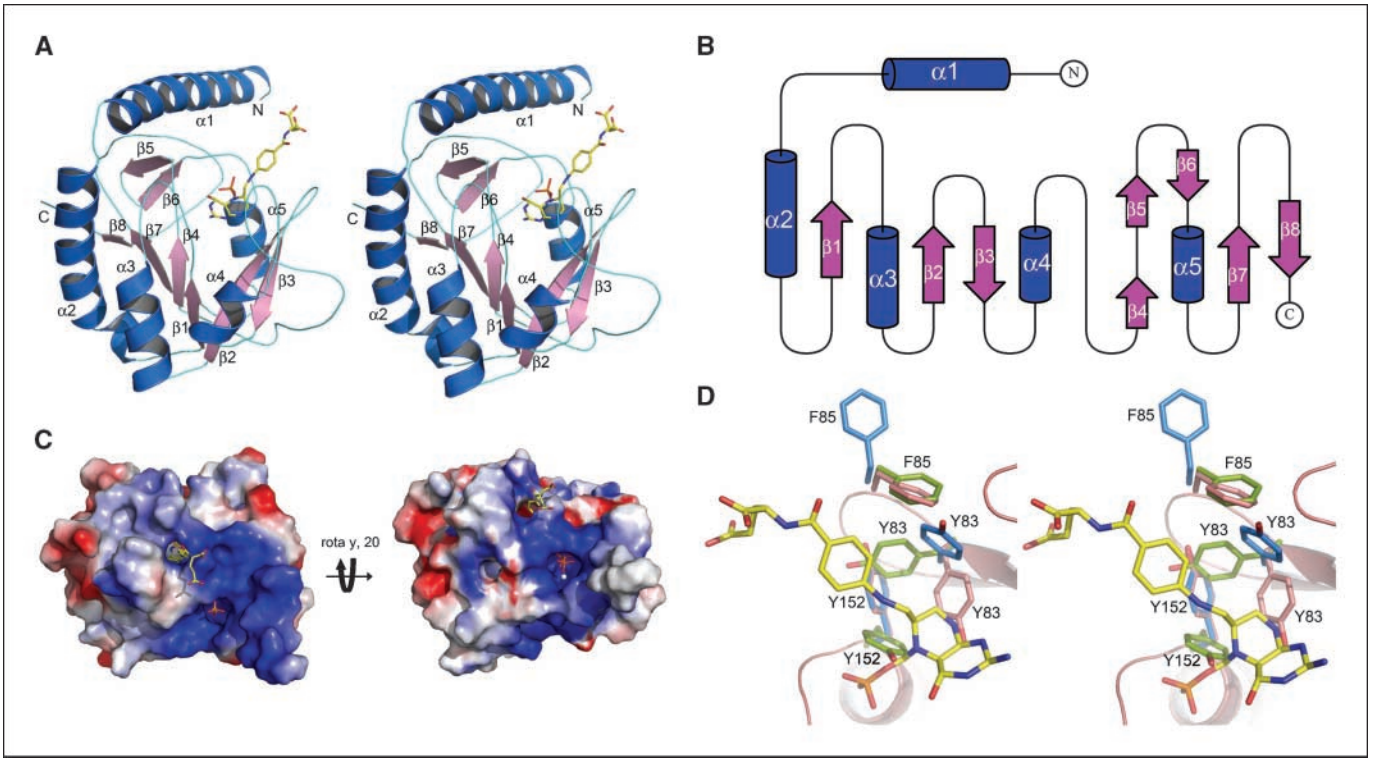

Figure 2. Structure of hMTHFS. *A,* stereo view of the hMTHFS structure as depicted by ribbon diagram. *N,* NH_2 terminus; *C,* COOH terminus. *B,* topology of hMTHFS. *C,* surface electrostatic potential representation of hMTHFS. *Blue,* positive potential; *red,* negative potential. The diphosphate and magnesium of the ADP-bound hMTHFS have been overlaid on the N5-iminium phosphate–bound hMTHFS. *Sticks,* N5-iminium phosphate and diphosphate; *sphere,* magnesium. *D,* conformational change of Y83, F85, and Y151 during catalysis. *Salmon, blue,* and *green sticks,* Y83, F85, and Y151 from native, intermediate, and enzyme-product complex, respectively; *yellow sticks,* intermediate.

the loop (A174-D193) region, part of which is disordered in the structure of the apoenzyme.

To gain a better understanding of the structural basis for substrate binding and the underlying mechanism of catalysis, we cocrystallized hMTHFS with ATP and 5-formyltetrahydrofolate. Interestingly, analysis of the electron density for the 5-formyltetrahydrofolate substrate, coupled with the results of a search for the anomalous signal of phosphate, revealed a phosphate group covalently linked to the carbon atom belonging to the formyl group of the 5-formyltetrahydrofolate. During the course of the cocrystallization (carried out at 16°C for 48 hours), the formyl group of the substrate seems to have completed a nucleophilic attack at the γ-phosphate of the ATP, resulting in the formation of the N5-iminium phosphate reaction intermediate, which was fortuitously trapped inside the crystal used for data collection. The structure of hMTHFS bound with the N5-iminium phosphate is similar to the structures of the apoenzyme and ADP-bound complex of hMTHFS. A notable difference is the movement of the side chain of Y83, which has implications on the catalysis (Fig. 2*D*).

The structure of the enzyme-product complex of hMTHFS was obtained by harvesting the crystals produced during the cocrystallization of hMTHFS with 5-formyltetrahydrofolate and ATP after 72 hours. Except for the conformation of the side chains of Y83, F85, and Y152, the overall structure of the enzyme-product complex of hMTHFS is similar to the native, ADP-bound, and N5-iminium phosphate–bound hMTHFS (Fig. 2*D*).

Folate binds in a spherical pocket. The pterin ring of the N5-iminium phosphate moiety sits in the center of a large spherical binding pocket formed by residues F55, L56, S57, M58, E61, P81, Y83, M90, W109, P135, R148, K150, Y152, and Y153 (Fig. 3*A*). The short helix (α4) and a long loop inserted between strands β3 and β4 act like a cap and are seen partially covering the active site. W109 is positioned above the pterin ring and seems to be closing the lid on the active site. The distance between the two aromatic rings is >7 Å, suggesting that W109 and the pterin ring do not interact. The conformation of the pterin ring is not planar. It is raised at the C6 position along the vertical axis (Fig. 3*B*). The twisting of the pterin ring probably helps bring the reacting functional groups in close proximity and adjust their orientation. The carboxyl oxygens of E61 are interacting with the N3 and amine nitrogens of the pterin ring. This interaction is of interest because the glutamic acid at this position is conserved in all the orthologs of MTHFS (Supplementary Fig. S1). M90 forms a hydrogen bond with the N8 nitrogen of the pterin ring. Numerous hydrophobic van der Waals contacts are observed between the pterin ring and the aromatic side chains of F55, Y83, P135, Y152, and Y153. Interestingly, the conformation of the aromatic ring of Y83 is distinctly different in the structures of native hMTHFS and N5-iminium phosphate–bound hMTHFS (Fig. 2*D*). The side chain swivels and occupies an upright position, which allows the pterin ring to dock in the binding pocket. This movement of the side chain of Y83 in turn displaces the side chain of F85 away from the binding pocket.

Further, the binding pocket is large enough to accommodate the pABA moiety of the substrate, which is almost perpendicular to the pterin ring. W109 and K150 form hydrogen bonds with the pABA ring. The glutamate protrudes out of the binding pocket through a circular hole at the top and is lying on the surface of the protein.

Adjacent to the hole is a large patch of positively charged potential, which may be involved in the binding of polyglutamates (Fig. 2*C*).

ATP binding site. hMTHFS contains an ATP binding site, which is distinct but in proximity to the substrate binding site (Figs. 2*C* and 3*A*). Based on the position of the phosphates, ATP binds in a positively charged cleft region between strand β6 and helix α5. The α- and β-phosphates are tethered in the ATP binding cleft by coordinate bonds with magnesium on one side and cohesive ionic bonds on the opposite side. K10 forms an ionic bond with the O2 atom of the α-phosphate, whereas R14 forms an ionic bond with the O1 atom of the β-phosphate. These residues are important for the docking of the ATP. The γ-phosphate forms two ionic bonds with R145. This interaction is critical for the correct orientation of the γ-phosphate in order for it to be able to mount a nucleophilic attack on the substrate and may also be essential for the stabilization of the intermediate. The ATP binding cleft is connected to the spherical tetrahydrofolate binding site internally through a channel such that the γ-phosphate of the ATP molecule is positioned close to the N5 atom of the pterin ring (Fig. 3*C*).

Enzyme-product complex. The structure of the enzyme-product complex was determined by delaying the harvest time of crystals obtained during cocrystallization of hMTHFS with 5-formyltetrahydrofolate and ATP. The overall structure of the hMTHFS bound with product is almost identical to the other structures of hMTHFS. Notably, the conformation of the side chains of Y83 and Y152 is distinctly different (Fig. 2*D*). In the structure of the N5-iminium phosphate–bound hMTHFS, we have seen that the aromatic ring of Y83 moves by 120° to make way for the substrate

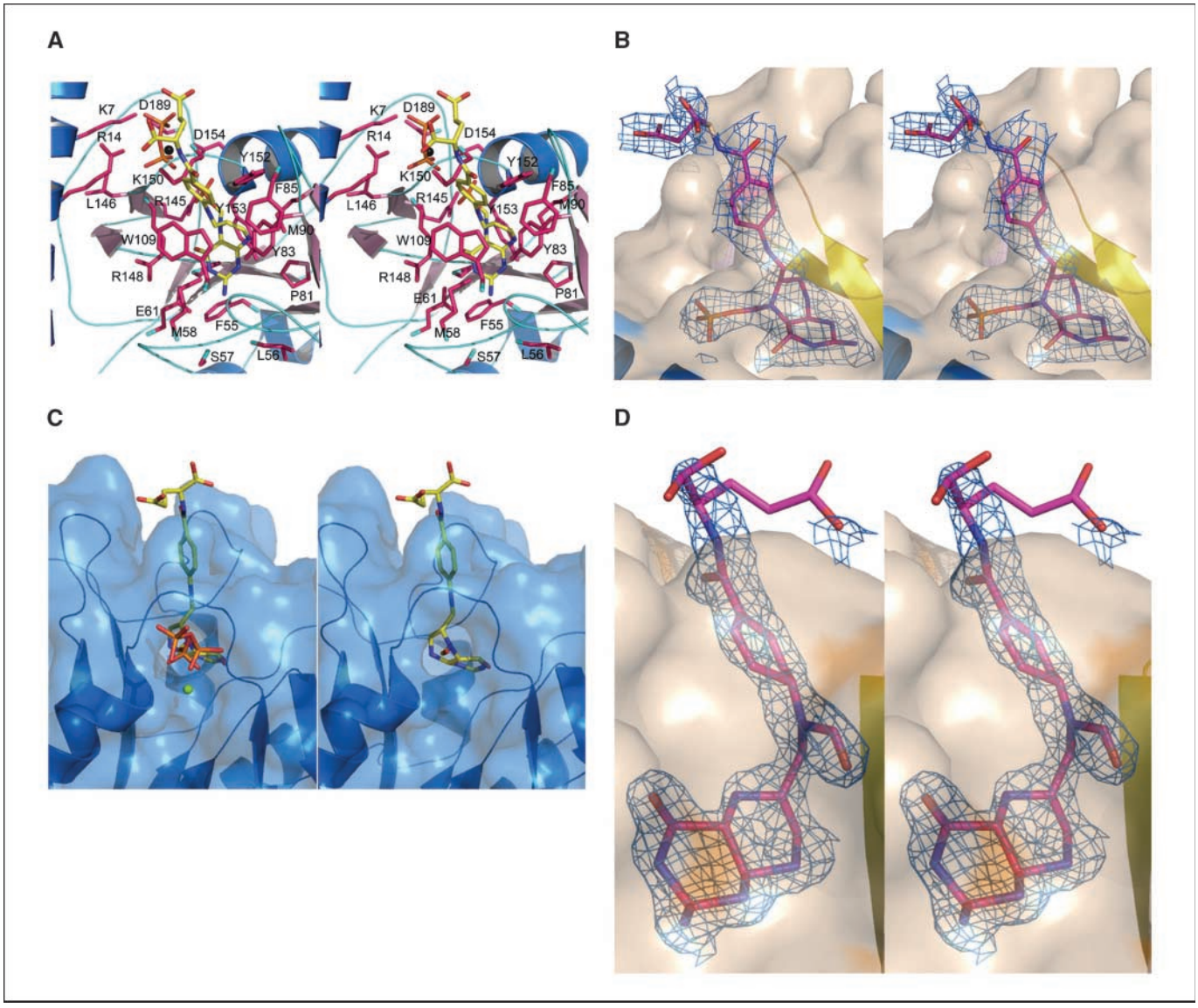

Figure 3. Active site of hMTHFS. *A,* the diphosphate (*sticks*) and magnesium (*sphere*) from the ADP-bound structure of hMTHFS were overlaid on the structure of N5-iminium phosphate–bound hMTHFS. *Magenta,* side chains of amino acids within hydrogen bonding and van der Waals distance of the N5-iminium phosphate (*yellow sticks*); *orange sticks,* diphosphate. *B,* stereo view of the 2*Fo-Fc* electron density for N5-iminium phosphate contoured at 2.0 σ. The map was calculated using a 2.8 Å resolution data set. *C,* cross-section of N5-iminium phosphate–bound hMTHFS depicting the channel connecting ATP binding site to the 5-formyltetrahydrofolate binding site. The phosphates and magnesium have been removed in the right panel. *D,* stereo view of the 2*Fo-Fc* electron density for 10-formyltetrahydrofolate at 1.0 σ. The map was calculated using a 1.8 Å resolution data set.

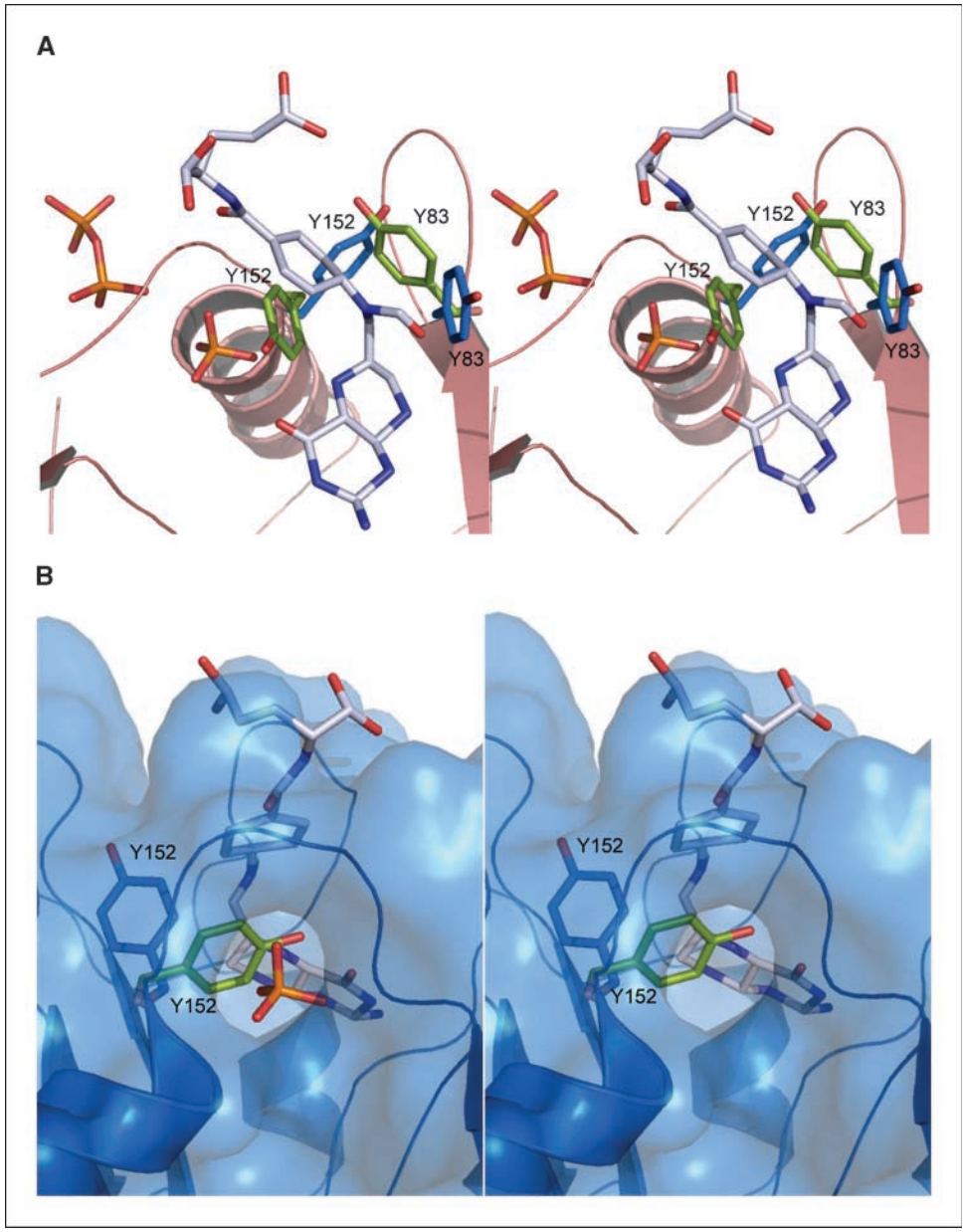

Figure 4. Structural basis for the inhibition of hMTHFS by 10-formyltetrahydrofolate. *A,* structural basis for the inhibition of hMTHFS by 10-formyltetrahydrofolate. The formyl group at N10 displaces Y83 (*blue sticks*) from its position seen in the reaction intermediate, which in turn displaces Y152. This obstructs the positioning of γ-phosphate as depicted by the overlaid phosphates from the ADP-bound hMTHFS structure. *B,* a cross-section of the surface view showing the obstruction of the channel connecting ATP binding site with the substrate binding site by Y152. The phosphate has been removed in the right panel for clarity. *Blue sticks,* Y83 and Y152 from the reaction intermediate; *green sticks,* their position in the product; *silver sticks,* 10-formyltetrahydrofolate.

to dock (Fig. 2*D*). In the enzyme-product complex, the aromatic ring of Y83 moves further 125° and is now seen forming a 2.4 Å hydrogen bond with the side chain nitrogen of N88. As a consequence of this movement, the aromatic ring of Y152 is displaced by 100° (Fig. 2*D*). The side chain of F85 seen displaced in the N5-iminium phosphate–bound hMTHFS structure returns back to its original position (Fig. 2*D*).

An interesting aspect of the study of the enzyme-product complex of hMTHFS was the analysis of the electron density for the product. The density was not continuous between the N5 and N10 atoms, and therefore, the product 5,10-methenyltetrahydrofolate could not be modeled. Instead, a formyl group could be modeled accurately in the extra density seen at the N10 position, suggesting the presence of 10-formyltetrahydrofolate rather than 5,10-methenyltetrahydrofolate in the active site of hMTHFS (Fig. 3*D*). 5,10-Methenyltetrahydrofolate has been reported to degrade non-enzymatically to 10-formyltetrahydrofolate previously (1, 34). Increasing the expression of MTHFS in SHSY-5Y cells increased the levels of 10-formyltetrahydrofolate to as much as 90% of the total cellular folate with a concomitant decrease in the levels of 5-formyltetrahydrofolate, suggesting that MTHFS may be able to catalyze the conversion of 5-formyltetrahydrofolate to 10-formyltetrahydrofolate (35). This is the first structural evidence for the synthesis of 10-formyltetrahydrofolate from 5-formyltetrahydrofolate by hMTHFS.

Structure-function analysis. Using the structures of hMTHFS as a guide, we selected and probed the role of residues surrounding the substrate and ATP binding site in catalysis by site-directed mutagenesis (Table 1). Wild-type and mutant hMTHFS were purified to homogeneity before testing the activity under identical conditions. We interpret and discuss the results of mutagenesis in light of the structures of hMTHFS, mpMTHFS, and bMTHFS. Equivalent positions for the hMTHFS residues in mpMTHFS and bMTHFS have been identified by superimposing the structures of

mpMTHFS and bMTHFS over the structure of hMTHFS. We extrapolate our findings to other orthologs of MTHFS by aligning the primary amino acid sequences obtained by running a PSI-BLAST search (36) for homologues of hMTHFS (Supplementary Fig. S1). Mutating K10, R14, or R145 to alanine decreased the enzyme activity dramatically (Table 1). The structure of hMTHFS in complex with ADP reveals that these residues are forming hydrogen bonds with the phosphates, implying that they are important for the binding of ATP. As expected, the D154A mutation almost completely abolished enzymatic activity. The OD1 and OD2 oxygens of D154 are hydrogen bonded to the magnesium ion and are part of the octahedral coordination shell of magnesium. This interaction is critical because the magnesium ion is hydrogen bonded to α- and β-phosphates of the ATP, which participates in the catalysis. K10, R14, R145, and D154 occupy identical positions in the hMTHFS, mpMTHFS, and bMTHFS structures. K10 and R14 are highly conserved, whereas R145 and D154 are absolutely conserved among orthologs of MTHFS (Supplementary Fig. S1). Thus, MTHFS tethers the phosphates of ATP using a highly conserved mechanism. The role of residues F55, E61, Y83, M90, Y153, M58, and R148 surrounding the pterin ring of tetrahydrofolate was investigated by mutating them to alanine (Table 1). Interestingly, the E61A and Y153A mutations almost completely abolished the enzymatic activity. In the structure of hMTHFS bound with N5-iminium phosphate, the carboxyl oxygens of E61 are interacting with the C2 amino group and the N3 nitrogen. These interactions are probably critical for anchoring the substrate in the binding pocket. Y153 is positioned below the pterin ring and defines the bottom edge of the binding pocket. Both E61 and Y153 are seen occupying identical positions in hMTHFS, mpMTHFS, and bMTHFS structures and are absolutely conserved in MTHFS orthologs (Supplementary Fig. S1). Although the M90A and R148A mutations did not abolish the enzymatic activity completely, >50% of the activity was compromised, indicating that the longer side chains at this position could increase the efficiency of catalysis of hMTHFS. M90 is replaced by an isoleucine in mpMTHFS. Interestingly, R148 has been changed to a phenylalanine and a tyrosine in mpMTHFS and bMTHFS, respectively. The arginine at this location is not highly conserved among the orthologs of MTHFS. Notably, the orthologs have only two choices at this position: an aromatic amino acid or an arginine (Supplementary Fig. S1). Because R148 is close to the pABA ring, replacing it with an aromatic amino acid could initiate stacking interactions with the pABA ring and promote the nucleophilic attack of N10 on the N5-iminium phosphate. The F55A mutation resulted in >45% loss in enzyme activity (Table 1), suggesting that a hydrophobic residue may be essential at this position for efficient catalysis. F55 is replaced by a tyrosine in mpMTHFS and a threonine in bMTHFS. Sequence alignment results reveal that this position is occupied by a hydrophobic residue in the orthologs of MTHFS. Y83 and M58 do not seem to be essential for catalysis because the enzyme activity did not decrease after mutating either of them to alanine. A valine is present at the position of Y83 in mpMTHFS, whereas a cysteine occupies an equivalent position in the structure of bMTHFS. M58 is replaced by an isoleucine in mpMTHFS. In the structure of native hMTHFS, F85 and W109 form a cap over the active site. The decrease in activity for the F85A mutation was only marginal. W109A mutation resulted in over 60% loss in activity (Table 1). These residues probably assist in isolating the reactants from the solvent during catalysis. A serine replaces the phenylalanine in mpMTHFS, whereas a lysine is seen at a similar position in bMTHFS. W109 is part of a long insertion (E96-G117), which is not seen in mpMTHFS. A tyrosine is present at a similar location in the bMTHFS. Further, the Y152A mutation lowered the enzyme activity by over 75% (Table 1). Y152 is close to the pterin ring and may be important for the correct orientation of the ring or the integrity of the binding pocket. The position of the side chain of Y152 is different in the native and enzyme-product complex structures of hMTHFS, suggesting a role for Y152 in product release. Y152 is conserved in the mpMTHFS and bMTHFS. A majority of the orthologs of MTHFS have a tyrosine at this position, with an occasional occurrence of phenylalanine (Supplementary Fig. S1). The K150A mutation did not have any effect on enzyme activity, suggesting that K150 is not essential for catalysis. K150 is replaced by a glycine in the bMTHFS.

Discussion

Determinants of ligand specificity. An interesting aspect of the native hMTHFS is the location of the side chain of Y83 inside the binding pocket. The aromatic ring of Y83 sterically obstructs the placement of the pterin ring inside the pocket (Fig. 2*D*). In the structure of the N5-iminium phosphate–bound hMTHFS, the side chain of Y83 has moved by 120°, allowing the placement of the pterin ring inside the pocket. Obviously, the Y83 somehow recognizes the substrate and moves. Such a mechanism of substrate binding offers greater selectivity by occluding functional groups that are not compatible or those that cannot be "recognized" by the side chain of Y83. Mutating Y83 to alanine had no effect on enzyme activity, suggesting that the role of Y83 is dispensable.

Structural basis for inhibition of hMTHFS by N10-substituted folate analogues. hMTHFS has been reported to be feedback inhibited by 10-formyltetrahydrofolate (22). Analysis of the structure of the enzyme-product complex of hMTHFS reveals that the synthesis or binding of 10-formyltetrahydrofolate places the formyl group of N10 within van der Waals radii of Y83. Therefore, to avoid steric clashes, Y83 moves by 125° from its position seen in the N5-iminium phosphate reaction intermediate-bound hMTHFS (Fig. 4*A* and *B*). The movement of Y83 displaces Y152, which moves away from Y83 to avoid steric clashes. This places Y152 in front of the channel connecting the ATP binding site with the substrate binding pocket. Y152 blocks the channel, obstructing any further nucleophilic attacks by the γ-phosphate of ATP (Fig. 4*A* and *B*). More importantly, the Y152 could preclude the positioning of the γ-phosphate of ATP within hydrogen bonding distance of N5 owing to steric hindrance. Therefore, tetrahydrofolates with N10 substitutions can act as potential inhibitors of MTHFS activity (23). Our study provides for the first time the structural basis for this inhibition. The structure of the N5-iminium phosphate–bound hMTHFS not only contributes toward the unraveling of the basis for this inhibition but also helps explain why Y83 may be unobtrusive during catalysis of 5-formyltetrahydrofolate to 5,10-methenyltetrahydrofolate. This further underscores the importance of having reaction intermediates while studying reaction mechanisms.

In conclusion, the structures of hMTHFS determined by us provide a clear picture of the folate and ATP binding pockets. The snapshot of the N5-iminium phosphate–bound hMTHFS accounts for the first intermediate formed during the conversion

of 5-formyltetrahydrofolate to 5,10-methenyltetrahydrofolate. The structure of the enzyme-product complex of hMTHFS reveals new features of hMTHFS-mediated catalysis. This study provides for the first time structural evidence for the synthesis of 10-formyltetrahydrofolate from 5-formyltetrahydrofolate by hMTHFS. From our structural studies, we can begin to rationalize the basis for inhibition of hMTHFS by 10-formyltetrahydrofolate and N10-substituted antifolates. We have identified amino acids critical for catalysis by site-directed mutagenesis. The structural, mutagenesis, and primary sequence analysis data of MTHFS orthologs suggest a highly conserved mechanism of catalysis. The structures of the essential hMTHFS reported here open up new opportunities for rationally designing antifolates or small molecules to combat the proliferation of cells.

Disclosure of Potential Conflicts of Interest

The authors declare they have no conflicts of interest.

Acknowledgments

Received 5/27/09; revised 6/26/09; accepted 7/9/09; published OnlineFirst 9/8/09.

Grant support: Ministry of Science and Technology of China grants 2006AA02A316, 2006CB910901, and 2009DFB30310; National Natural Science Foundation of China grants 30870483, 30670427, and 30721003; Ministry of Health of China grant 2008ZX10004-015; and CAS Research grant KSCX2-YW-R-127.

The costs of publication of this article were defrayed in part by the payment of page charges. This article must therefore be hereby marked *advertisement* in accordance with 18 U.S.C. Section 1734 solely to indicate this fact.

We thank Xudong Zhao of the core facilities center at IBP for technical assistance.

Crystallographic data were collected at the Structural Biology Center beamline 19-ID (Advanced Photon Source, Argonne National Laboratory) and the Shanghai Synchrotron Radiation Facility beamline BL17U.

References

1. Appling DR. Compartmentation of folate-mediated one-carbon metabolism in eukaryotes. FASEB J 1991;5:2645–51.

2. Fox JT, Stover PJ. Folate-mediated one-carbon metabolism. Vitam Horm 2008;79:1–44.

3. Farber S, Diamond LK, Mercer RD, Sylvester RF, Wolff VA. Temporary remission in acute leukemia in children produced by folic acid antagonist, 4-aminopteroyl glutamic acid (aminopterin). N Engl J Med 1948;238:787–93.

4. Chattopadhyay S, Moran RG, Goldman DI. Pemetrexed: biochemical and cellular pharmacology, mechanisms, and clinical applications. Mol Cancer Ther 2007;6:404–17.

5. Pui CH, Evans WE. Treatment of acute lymphoblastic leukemia. N Engl J Med 2006;354:166–78.

6. Longley DB, Harkin DP, Johnston PG. 5-Fluorouracil: mechanisms of action and clinical strategies. Nat Rev Cancer 2003;3:330–8.

7. Carreras CW, Santi DV. The catalytic mechanism and structure of thymidylate synthase. Annu Rev Biochem 1995;64:721–62.

8. Sirotnak FM, Wendel HG, Bornmann WG, et al. Coadministration of probenecid, an inhibitor of a cMOAT/MRP-like plasma membrane ATPase, greatly enhanced the efficacy of a new 10-deazaaminopterin against human solid tumors *in vivo*. Clin Cancer Res 2000;6:3705–12.

9. Bertino JR. "Rescue" techniques in cancer chemotherapy: use of leucovorin and other rescue agents after methotrexate treatment. Semin Oncol 1977;4:203–16.

10. Renwick SB, Snell K, Baumann U. The crystal structure of human cytosolic serine hydroxymethyltransferase: a target for cancer chemotherapy. Structure 1998;6:1105–16.

11. Schirch V, Szebenyi DM. Serine hydroxymethyltransferase revisited. Curr Opin Chem Biol 2005;9:482–7.

12. Stover P, Schirch V. Serine hydroxymethyltransferase catalyzes the hydrolysis of 5,10-methenyltetrahydrofolate to 5-formyltetrahydrofolate. J Biol Chem 1990;265:14227–33.

13. Allegra CJ, Drake JC, Jolivet J, Chabner BA. Inhibition of phosphoribosylaminoimidazolecarboxamide transformylase by methotrexate and dihydrofolic acid polyglutamates. Proc Natl Acad Sci U S A 1985;82:4881–5.

14. Piper JR, McCaleb GS, Montgomery JA, et al. Synthesis and antifolate activity of 5-methyl-5,10-dideaza analogues of aminopterin and folic acid and an alternative synthesis of 5,10-dideazatetrahydrofolic acid, a potent inhibitor of glycinamide ribonucleotide formyltransferase. J Med Chem 1988;31:2164–9.

15. Jolivet J. Human 5,10-methenyltetrahydrofolate synthetase. Methods Enzymol 1997;281:162–70.

16. Huennekens FM, Henderson GB, Vitols KS, Grimshaw CE. Enzymatic activation of 5-formyltetrahydrofolate via conversion to 5, 10-methenyltetrahydrofolate. Adv Enzyme Regul 1984;22:3–13.

17. Jolivet J, Dayan A, Beauchemin M, Chahla D, Mamo A, Bertrand R. Biochemical and molecular studies of human methenyltetrahydrofolate synthetase. Oncologist 1996;1:248–53.

18. Maras B, Stover P, Valiante S, Barra D, Schirch V. Primary structure and tetrahydropteroylglutamate binding site of rabbit liver cytosolic 5,10-methenyltetrahydrofolate synthetase. J Biol Chem 1994;269:18429–33.

19. Huang T, Schirch V. Mechanism for the coupling of ATP hydrolysis to the conversion of 5-formyltetrahydrofolate to 5,10-methenyltetrahydrofolate. J Biol Chem 1995;270:22296–300.

20. Chen S, Yakunin AF, Proudfoot M, Kim R, Kim SH. Structural and functional characterization of a 5,10-methenyltetrahydrofolate synthetase from *Mycoplasma pneumoniae* (GI: 13508087). Proteins 2005;61:433–43.

21. Meier C, Carter LG, Winter G, Owens RJ, Stuart DI, Esnouf RM. Structure of 5-formyltetrahydrofolate cycloligase from *Bacillus anthracis* (BA4489). Acta Crystallogr Sect F Struct Biol Cryst Commun 2007;63:168–72.

22. Field MS, Szebenyi DM, Stover PJ. Regulation of *de novo* purine biosynthesis by methenyltetrahydrofolate synthetase in neuroblastoma. J Biol Chem 2006;281:4215–21.

23. Field MS, Szebenyi DM, Perry CA, and Stover PJ. Inhibition of 5,10-methenyltetrahydrofolate synthetase. Arch Biochem Biophys 2007;458:194–201.

24. Berman HM, Bhat TN, Bourne PE, et al. The Protein Data Bank and the challenge of structural genomics. Nat Struct Biol 2000;7:957–9.

25. Stols L, Gu M, Dieckman L, Raffen R, Collart FR, Donnelly MI. A new vector for high-throughput, ligation-independent cloning encoding a tobacco etch virus protease cleavage site. Protein Expr Purif 2002;25:8–15.

26. Otwinowski Z, Minor W. Processing of X-ray diffraction data collected in oscillation mode. Methods Enzymol 1997;276:307–26.

27. Long F, Vagin A, Young P, Murshudov GN. BALBES: a molecular-replacement pipeline. Acta Crystallogr D Biol Crystallogr 2008;64:125–32.

28. McCoy AJ, Grosse-Kunstleve RW, Adams PD, Winn MD, Storoni LC, Read RJ. Phaser crystallographic software. J Appl Cryst 2007;40:658–74.

29. Adams PD, Grosse-Kunstleve RW, Hung LW, et al. PHENIX: building new software for automated crystallographic structure determination. Acta Crystallogr D Biol Crystallogr 2002;58:1948–54.

30. Murshudov GN, Vagin AA, Dodson EJ. Refinement of macromolecular structures by the maximum-likelihood method. Acta Crystallogr D Biol Crystallogr 1997;53:240–55.

31. Brünger AT. Free R value: a novel statistical quantity for assessing the accuracy of crystal structures. Nature 1992;355:472–5.

32. Emsley P, Cowtan K. Coot: model-building tools for molecular graphics. Acta Crystallogr D Biol Crystallogr 2004;60:2126–32.

33. Davis IW, Murray LW, Richardson JS, Richardson DC. MOLPROBITY: structure validation and all-atom contact analysis for nucleic acids and their complexes. Nucleic Acids Res 2004;32:615–9.

34. May M, Bardos TJ, Barger FL, et al. Synthetic and degradative investigations of the structure of folinic acid-SF. J Am Chem Soc 1951;73:3067–75.

35. Girgis S, Suh JR, Jolivet J, Stover PJ. 5-Formyltetrahydrofolate regulates homocysteine remethylation in human neuroblastoma. J Biol Chem 1997;272:4729–34.

36. Altschul SF, Madden TL, Schäffer AA, et al. Gapped BLAST and PSI-BLAST: a new generation of protein database search programs. Nucleic Acids Res 1997;25:3389–402.

37. Larkin MA, Blackshields G, Brown NP, et al. Clustal W and Clustal X version 2.0. Bioinformatics 2007;23:2947–8.